15

Analysis of CZTSSe Monograin Layer Solar Cells

Gregor Černivec, Andri Jagomägi and Koen Decock
[1]*University of Ljubljana, Faculty of Electrical Engineering,*
[2]*Department of Materials Science, Tallinn University of Technology,*
[3]*Solar Cells Department, Ghent University – ELIS,*
[1]*Slovenia*
[2]*Estonia*
[3]*Belgium*

1. Introduction

Monograin layer (MGL) solar cell combines the features of a monocrystalline solar cell and a thin film solar cell. The photoactive layer is formed from the kesterite-stannite semiconductor $Cu_2SnZn(S,Se)_4$ (CZTSSe) material with the single-crystalline grains embedded into the epoxy resin (Altosaar et al., 2003). With the graphite back contact, cadmium sulphide (CdS) buffer layer, and zinc oxide (ZnO:Al/i-ZnO) window layer, the remainder of the structure resembles a thin film CIS solar cell in the superstrate configuration (Fig. 1).

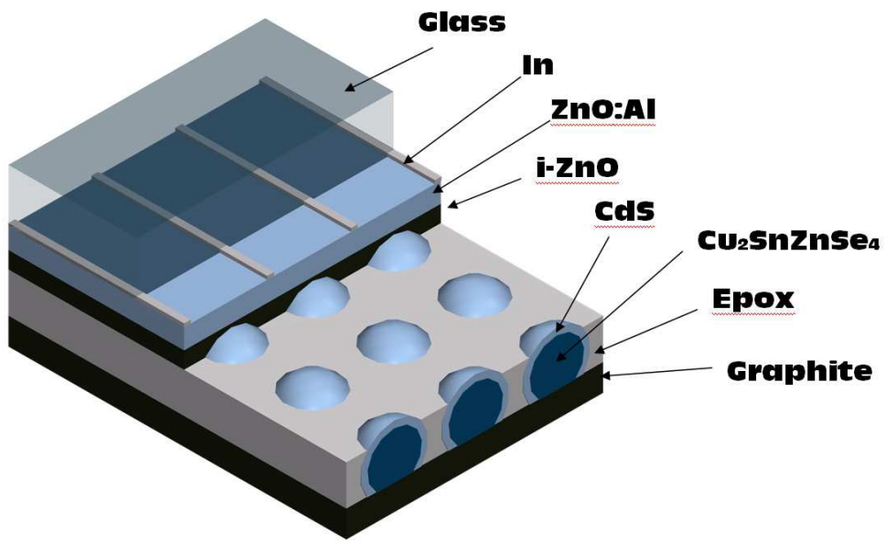

Fig. 1. The MGL solar cell. The photoactive $Cu_2SnZnSe_4$ monograins are covered with CdS, and embedded into the epoxy resin. The thin layer of the intrinsic ZnO serves as the CdS surface passivation and as the barrier for the ZnO:Al impurities. The front contact comprises indium fingers while the back contact is made of the graphite paste.

The main advantage of this cell over the thin film CIGS solar cell are the low production costs – using a relatively simple powder technology (Altosaar et al., 2005), and the replacement of the expensive indium (In) by the less expensive tin (Sn) and zinc (Zn) metals. The photovoltaic properties of this new structure are very promising: the AM1.5 spectrum conversion efficiency reaches up to 5.9% along with the open-circuit voltage (V_{oc}) up to 660 mV and the fill-factor (*FF*) up to 65%. The short-circuit current (J_{sc}) has its maximal value at the room temperature and then decreases with the lowering temperature. Along with the low *FF*, these output parameters point to some specific charge transport properties.
In order to discover the origin of the charge transport limiting mechanism we employed the numerical semiconductor simulator Aspin (Topič et al.,1996), based on the drift-diffusion equations (Selberherr, 1984) and coupled to the SRH (Schockley & Read, 1952) recombination statistics. The optical generation rate profile was calculated with the ray tracing simulator Sun*Shine* (Krč et al., 2003), which is able to determine the absorption profile in the illuminated one-dimensional (1D) structure that comprises a stack of layers with flat and/or rough adjacent interfaces. The input semiconductor material parameters were determined from the temperature resolved admittance spectroscopy measurements (Walter et al.,1996): capacitance-voltage (*C-V*) and capacitance-frequency (*C-f*), the van der Pauw measurement (Van der Pauw, 1958) and the dark current density-voltage (*J-V*) characteristics measurements (Sah et al., 1957). The numerical model was implemented in a similar way as in (Černivec et al., 2008) where the measured parameters were used as the input and the *J-V* and the external quantum efficiency (*QE*) characteristics were the result of the simulation. By comparing the temperature dependent output characteristics of the AM1.5 illuminated solar cell to the measurements, and additional fine tuning of the input parameters, we assumed the plausible efficiency-limiting mechanism, and by that also revealed the region in the structure that could be responsible for the charge transport limitations.

2. Input parameters measurements

In order to extract material parameters which will be further on used in the numerical analysis, following measurements were conducted: the dark *J-V* measurement to get insight into the recombination and transport properties of the solar cell, the *C-V* measurement which indicates the width and the shape of the junction, and the *C-f* measurement which results the information of the defect properties of the semiconductor material. The common assumption in the analyses of the measurements is a single-junction model of the solar cell. In the interpretation of the Van der Pauw measurement results we assumed a similar morphology of the annealed tablet of the CZTSSe material as it is one in the solar cell's monograin absorber.

2.1 One-diode model

Calibration of the parameters of the one-diode model does not yield any input parameters for our numerical model, but it rather gives us initial insight into the transport properties of the MGL solar cell. Table I contains the extracted temperature dependent parameters of the fitted one-diode model (Sze & Ng, 2007). The high ideality factors (n_{id}) of the temperature dependent dark *J-V* measurement indicate the CdS/CZTSSe heterointerfacial limited transport.

T [K]	J_0 [mA/cm²]	n_{id} [/]	R_s [Ωcm²]	G_{sh} [mS/cm²]
310	1.08x10^{-3}	2.68	2.10	0.23
290	4.85x10^{-4}	2.78	2.36	0.17
270	2.50x10^{-4}	2.99	2.66	0.12
250	8.93x10^{-5}	3.19	3.44	0.083
230	3.30x10^{-5}	3.37	4.37	0.061
210	1.44x10^{-5}	3.78	6.65	0.033

Table 1. Parameters of the fitted one-diode model.

The ideality factors above 2 deviate from the standard Sah-Noyce-Shockley theory (Sah et al., 1957) and point either to the tunnelling enhanced recombination in the space charge region (SCR) (Dumin & Pearson, 1965) or to the multilevel recombination (Breitenstein et al., 2006; Schenk et al., 1995) occurring in the highly defective interfacial regions.

Fig. 2 shows the Arrhenius plot of the dark saturation current (J_0) and its extracted activation energy ($E_{A,\,J0}$). The activation energy is the distance between the Fermi level and the edge of the minority carrier energy band, since these are responsible for the recombination current. In the case of the MGL solar cell, at the CdS/CZTSSe heterointerface the inverted surface makes holes to be the minority carriers, Fig. 8. Thus the $E_{A,\,J0}$ represents the energy distance between the CZTSSe absorber's valence band and the Fermi level near the heterointerface.

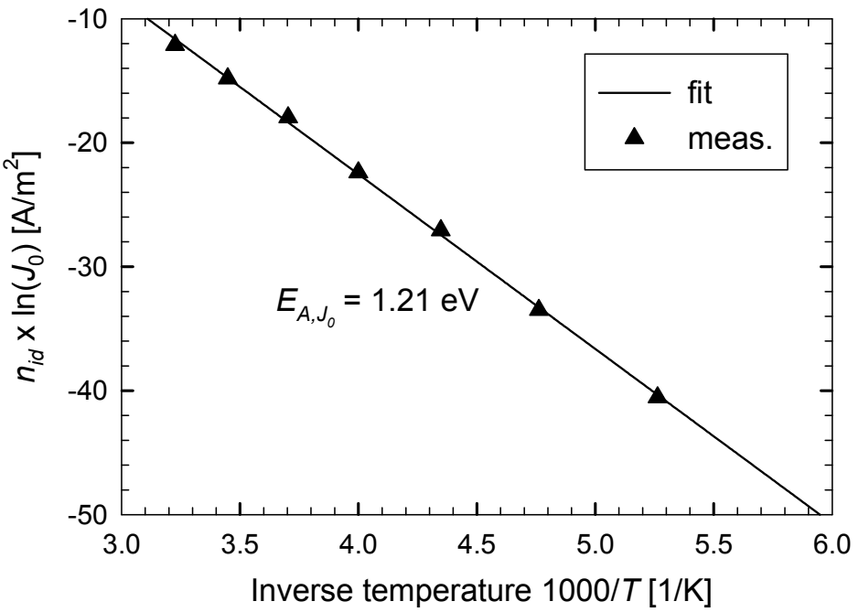

Fig. 2. Arrhenius plot of the dark saturation current as obtained from the one-diode model. The slope of the ideality factor weighted logarithm of the dark saturation current versus the inverse absolute temperature, results the activation energy $E_{A,\,J0}$. T is temperature in Kelvin.

Comparing the value of the $E_{A,\,J0}$ (Fig. 2) to the absorber's band-gap energy as extracted from the QE measurement (Fig. 13, $E_{g,CZTSSe}$ = 1.49 eV), this indicates the position of the recombination peak near the heterointerface and inside the SCR – as depicted in Fig. 8.

2.2 Capacitance-voltage measurement

To obtain the approximate values of the concentration of the uncompensated acceptors (Kosyachenko, 2010) at the edge of the SCR, and the hole mobility ($\mu_{h,CZTSSe}$) of the CZTSSe absorber layer, we combined the temperature resolved *C-V* and the van der Pauw measurements. Since the concentration of the uncompensated acceptors at the edge of the SCR corresponds to the density of free holes, we will further on introduce this as new parameter called the "apparent doping" – p_{SCR}.

Fig. 3 shows the temperature and the bias voltage dependent capacitance plot – the Mott-Schottky plot, where the capacitance results from the admittance measurement at 10 kHz. The nonlinear curves in the Mott-Schottky plot indicate a spatially non-uniform p_{SCR}, while their temperature trend points to the temperature decreasing capacitance. The slope of the curves at V = 0 V indicates that, in dark conditions, the apparent doping at the edge of the SCR gradually increases with the decreasing temperature.

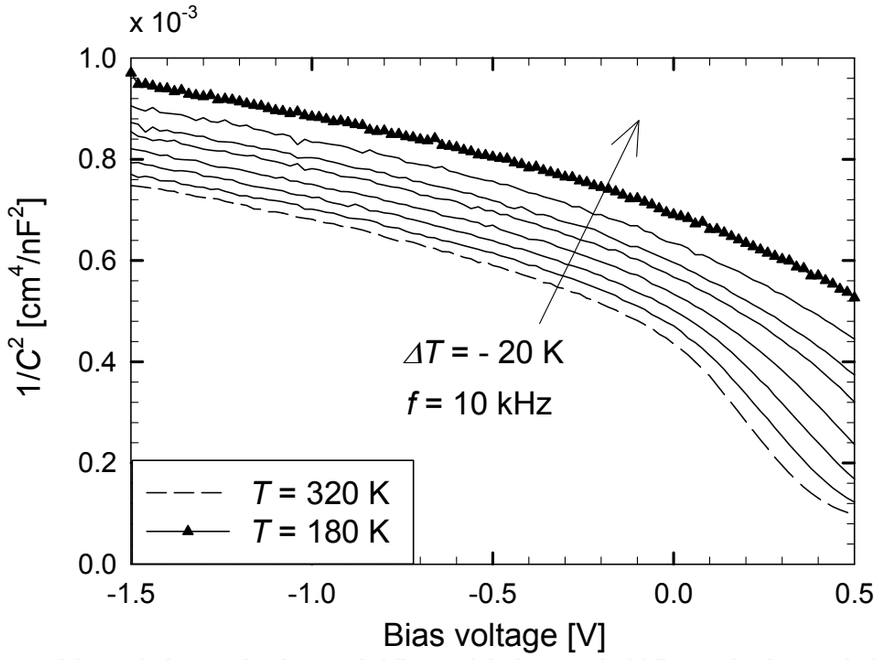

Fig. 3. The Mott-Schottky plot at 10 kHz. The dashed curve correlates to the temperature at 320 K. Arrow indicates the trend of the temperature decrement. The temperature step equals to 20 K. All curves are measured with a small signal of 10 kHz.

When we observe the 0V bias points as depicted in Fig. 4 by the triangles, we can see that p_{SCR} decreases when moving from the quasi-neutral region towards the SCR. However, for the higher temperatures (320 K, 300 K) p_{SCR} seems to be increasing towards the heterointerface after it has reached its minimum value. We are not able to explain this trend properly, but since the increasing p_{SCR} towards the heterointerface would produce only a poor photovoltaic junction, in the modelling we use the p_{SCR} values as obtained at 0 V bias. The trend of the increasing SCR width along with the increasing p_{SCR} could results from the influences of the non-ideally asymmetrical n^+/p (CdS/CZTSSe) junction in which the SCR extends also into the n^+ buffer region (CdS).

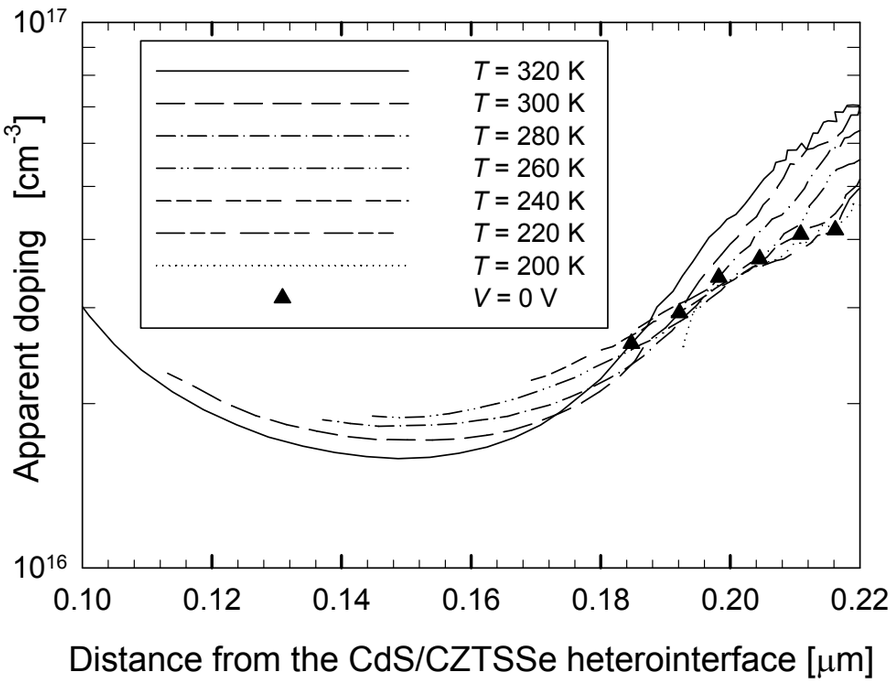

Fig. 4. The apparent doping density p_{SCR} obtained from the bias voltage derivative of the Mott-Schottky plot. The distance from the junction is calculated from the space charge region capacitance. Triangles depict the 0 V bias conditions.

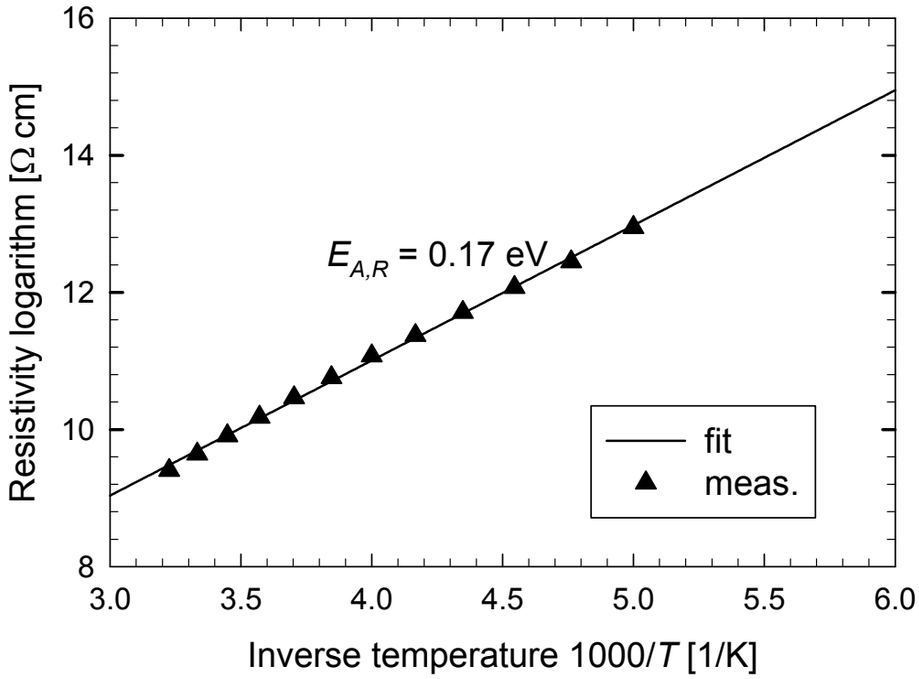

Fig. 5. Arrhenius plot of the van der Pauw measurement conducted on the annealed CZTSSe tablet. $E_{A,R}$ is the extracted activation energy. T is temperature in Kelvin.

2.3 Van der Pauw measurement

The van der Pauw measurements were conducted on the tablet of the annealed CZTSSe monograin material. The Arrhenius plot of the resistivity (ρ) of the monograin material tablet (Fig. 5) reveals the thermal activation energy ($E_{A,R}$) equal to 0.17 eV, and a very low hole mobility $\mu_{h,CZTSSe}$ equal to 0.02 cm²/Vs at 310 K. The latter was calculated according to (1) and using the p_{SCR} as obtained from the *C-V* profiling:

$$\mu_{h.CZTSSe} = \frac{1}{q \cdot p_{SCR} \cdot \rho}. \tag{1}$$

2.4 Capacitance-frequency measurement

Plotting the capacitance as a function of the measurement frequency on a semi-logarithmic scale can reveal some defects present in the energy gap of the CZTSSe absorber layer of the MGL solar cell. A gradually decaying capacitance indicates a defect with a broad energy band, while a steep transition indicates a single level defect (Burgelman & Nollet, 2005). The temperature resolved *C-f* plot shown in Fig. 6 reveals both types of transitions: a gradually decreasing capacitance at the high temperature limit (indicated with triangles), and a characteristic inflection point at the frequency equal to 10 kHz in the low temperature limit (indicated with circles).

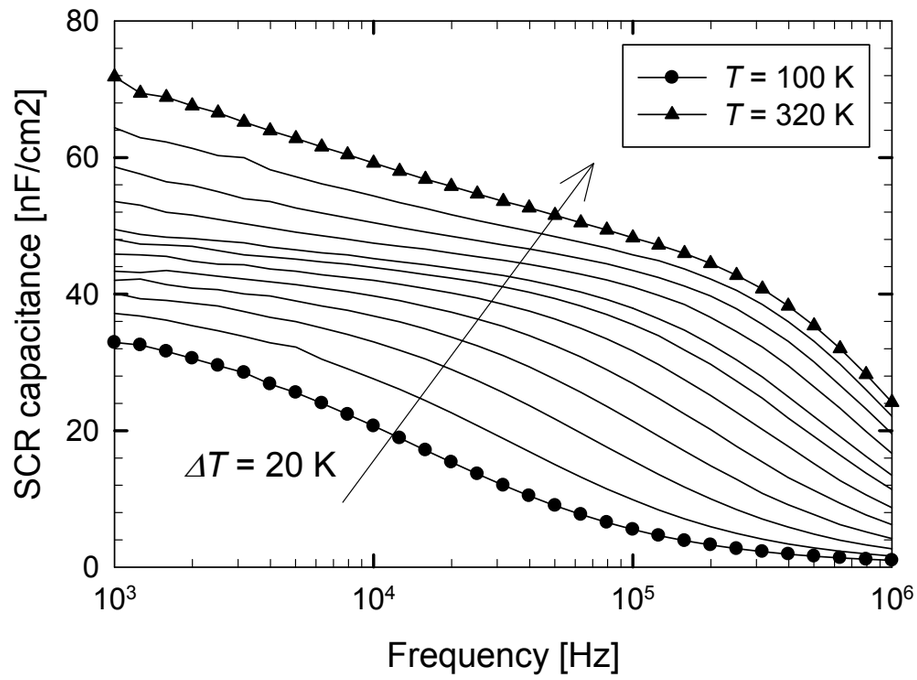

Fig. 6. Frequency dependent space charge region's capacitance measured at 0.2 V of forward bias. Solid curve with circles depicts the relation at 100 K. The arrow indicates the trend of the curves with the increasing temperature. The temperature step equals to 20 K. The curves at lower temperatures exhibit pronounced inflection points thus indicate emission from shallow traps.

The decreasing capacitance going from the high temperature towards the low temperature indicates the 'freeze out' of the carriers located in the deep traps: the temperature shrinking of the Fermi distribution tail makes the deep trapped charge less sensitive to the small perturbations of the Fermi level (the applied ac signal). The analysis according to (Walter et al.,1996) reveals two trap distributions which are shown in Fig. 7. Measurement at room temperature senses a broad trap distribution extending at least 0.3 eV deep into the energy gap from the valence band, while the measurement at low temperature fingers a very narrow distribution with its maximum at 0.05 eV. Since this maximum remains present also at high reverse biases (not shown here), we believe that this trap extends throughout the whole CZTSSe absorber layer and acts as the intrinsic acceptor doping level. However we can not draw any strong conclusions on the type of the deep trap distribution, but since this could be responsible for the compensating effect; we postulated it to be the donor-like.

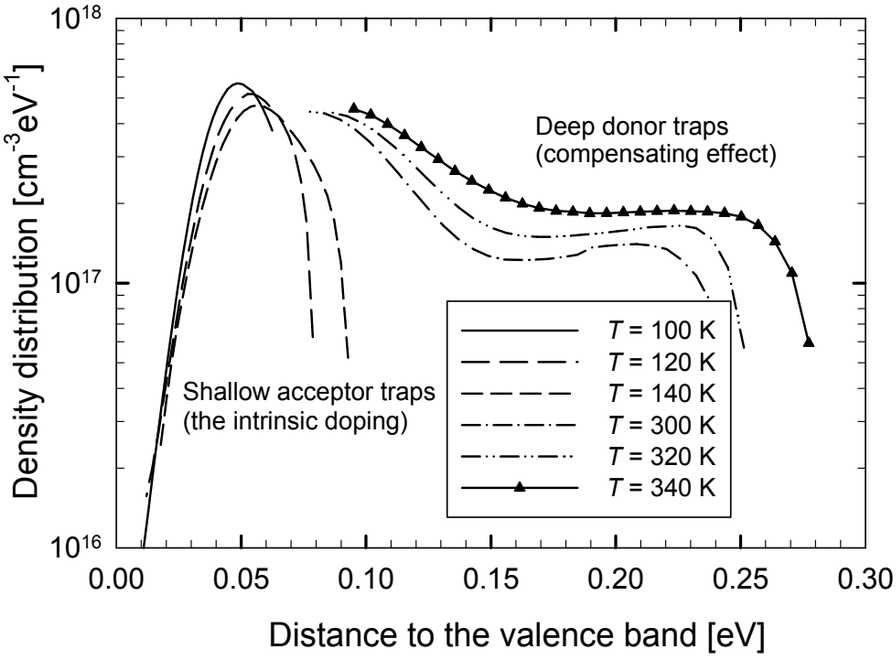

Fig. 7. Trap density distributions extracted at 0.2 V of forward bias calculated as the frequency derivative of the space charge region's capacitance. Calibration parameters were chosen according to (Walter et al.,1996): U_d = 0.8 V (built-in voltage), $\beta_p N_V$ = 5x10^7 Hz (trap emission coefficient), E_{fp} = 0.7 eV (the Fermi level position relating the valence band), 1x10^3 ≤ f ≤ 1x10^6 Hz (frequency range).

In Fig. 7 the pronounced narrow distribution at 0.05 eV above the valence band indicates the shallow acceptor traps responsible for the intrinsic doping, while the deeper and wider donor distribution (marked with triangles) results the compensation effect.

3. Modelling

From the measurements we obtained a certain insight into the recombination and transport properties (the dark *J-V* and the Van der Pauw measurements), the doping profile (*C-V* measurement) and the indication of the shallow traps (*C-f* measurement). These will be used as the guidelines to define the numerical model of the CZTSSe MGL solar cell.

The 1D carrier transport model can accurately describe the current flow only in the direction vertical to the layered structure (the direction orthogonal to the solar cell plane) therefore following assumptions are made: i) current flow in the matrix plane between the adjacent monograins is neglected, ii) all the semiconductor parameters are meant as the "effective parameters", thus neglecting the morphology by transforming a single spherical monograin solar cell into the 1D rod, and iii) the "spatial fill-factor" (S_{FF}) is introduced, which is the ratio of the grain covered area to the whole contact area. It is important to note that the S_{FF} affects only the extensive solar cell parameters (J_{sc}) while the intensive parameters (V_{oc}, FF and QE) remain intact. In our case the S_{FF} equals to 0.78.

The most important semiconductor parameters which have to be defined for each layer of the MGL solar cell prior to simulation are the band-gap energy (E_g), the electron affinity (E_χ), the acceptor and/or donor doping (N_A, N_D), the hole and electron low-field mobility (μ_h, μ_e), the hole and electron effective masses (m_h, m_e), and the parameters of the traps and/or the recombination centres (N_t – distribution density, E_t – distance to the valence band, σ – trap cross section, e_t – characteristic energy). By analyzing the conducted measurements (*C-V*, van der Pauw, *C-f*) we extracted the initial values of these parameters, relating to the CZTSSe absorber and/or to the CdS/CZTSSe heterointerface. These were further on subjected to the calibration procedure in order to fit the dark structure and the illuminated structure output characteristics to the measurements (*J-V* and *QE*). The rest of the absorber and heterointerface parameters, and those relating to the window (ZnO:Al/ZnO) and buffer (CdS) layers of the MGL solar cell, were taken similar to those used in (Černivec et al., 2008).

3.1 Dark structure *J-V* characteristics

Fig. 8 shows the CZTSSe MGL solar cell structure in its thermodynamic equilibrium. The complete solar cell comprises glass(2 mm)/ZnO:Al(1.6 μm)/i-ZnO(200 nm)/CdS(50 nm)/CZTSSe(60 μm)/graphite(500 nm) layers with the additional 100 nm thick surface

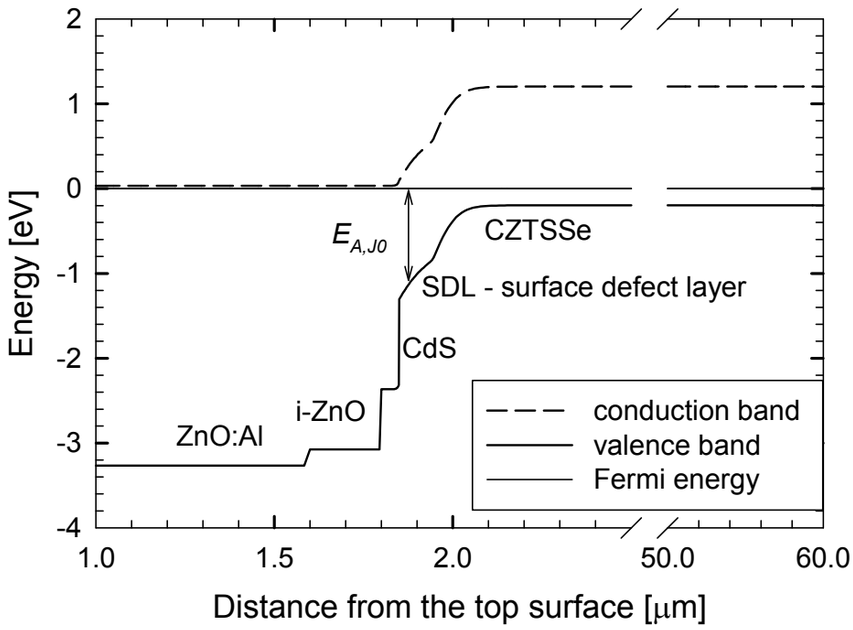

Fig. 8. Energy band diagram of CZTSSe solar cell in thermodynamic equilibrium at 310 K. $E_{A,J0}$ indicates the recombination activation energy as obtained from the Arrhenius plot from Fig. 2.

defect layer (SDL) between the CdS and the CZTSSe to account for the interfacial defects. Because of the degenerate position of the Fermi level in the ZnO:Al, i-ZnO and CdS layers, we assume these will act as the emitter contact, while the graphite at the back acts as the ohmic base contact. Further on in the structure we introduce the SDL which has an increased concentration of the mid-gap defects of the donor ($N_{tD,SDL}$) and the acceptor ($N_{tA,SDL}$) types. $N_{tD,SDL}$ will be responsible for the recombination current while the $N_{tA,SDL}$ will set the Fermi level position in the SDL layer and thus activate the $N_{tD,SDL}$.

The van der Pauw measurements of the sole CZTSSe tablets exhibit unusual high resistances, thus we assume that $\mu_{h,CZTSSe}$ will have an important impact to the series resistance – R_s (Table I). The Arrhenius plot in Fig. 5 shows the latter's exponential dependence on temperature, revealing the activation energy of 0.17 eV. We believe that the high R_s originates from the compensation of the shallow acceptor doping ($N_{tA,CZTSSe}$) by the broader distribution of deeper donor levels ($N_{tD,CZTSSe}$). This agrees well with the *C-f* measurement results shown in Fig. 7. Therefore, rather than calculating the mobility from the van der Pauw measurement, we will use a numerical fitting procedure to calibrate the $\mu_{h,CZTSSe}$ and the $N_{tD,SDL}$ for the preselected values of the $N_{tA,CZTSSe}$ and the $N_{tD,CZTSSe}$. The initial values for the latter two were calculated from the *C-f* measurement (Fig. 7).

Fig. 9 shows the calibration procedure of the measured and the simulated dark *J-V* characteristics at 310 K. By increasing the total concentration of the SDL mid-gap donor defects ($N_{tD,SDL}$) the dark saturation current increases, as shows the inset of Fig. 9. In the voltage range from 0.4 V to 0.6 V a good *J-V* fit can be found for the $N_{tD,SDL}$ equal to 10^{18} cm^{-3}, but still expressing a deviation in the slope as the result of the non-matching ideality factors: with this model it is not possible to obtain such a high ideality factor as yielded the measurement-calibration in Table I. For the lower applied voltages (V < 0.4 V) there is a significant deviation in characteristics which can be attributed to the shunt conductance. To compensate this difference the external shunting element can be added in the model, using the value equal to the G_{sh} at 310 K (Table I). A very good fit is found in the voltage range V > 0.5 V by setting the value of the $\mu_{h,CZTSSe}$ to 1.5 cm^2/Vs – indicated by the solid line in Fig. 9.

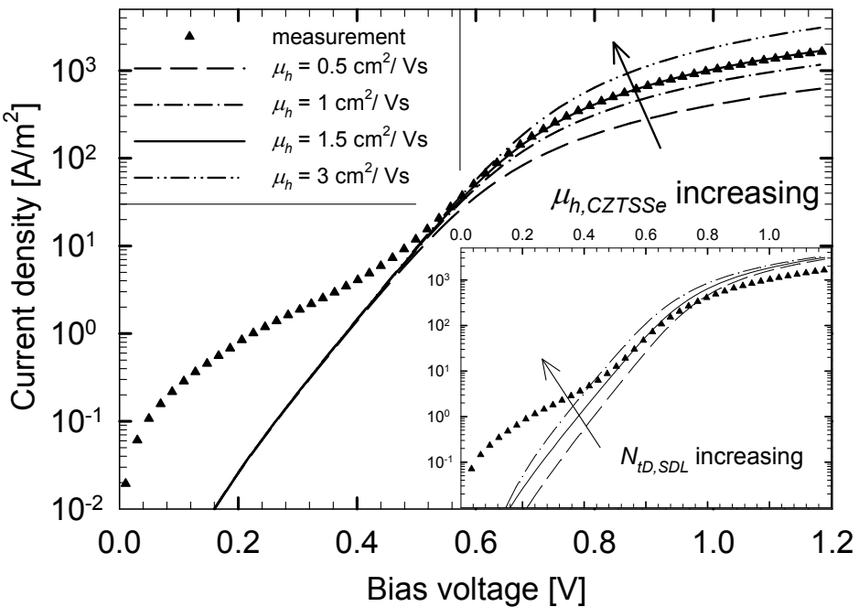

Fig. 9. Calibration of the CZTSSe monograin layer's and of the SDL's transport parameters.

In Fig. 9 the calibrated value of the CZTSSe hole mobility equals to 1.5 $cm^2(Vs)^{-1}$ and the corresponding electron mobility equals to 8 $cm^2(Vs)^{-1}$. The inset of Fig 9 shows calibration of the SDL defect concentration. The calibrated defect concentration ($N_{tD,SDL}$ = 8x10^{19} cm^{-3}/eV) corresponds to the solid *J-V* curve of the three simulated characteristics. The *J-V* curve above (dash-dotted) and the *J-V* curve below (dashed) correspond to one order of magnitude higher and to one order of magnitude lower SDL defect concentration, respectively.
To summarize the dark model, this is valid for the bias voltages higher than 0.5 V. When the solar cell is illuminated, this usually happens to be the range at which the recombination current starts to compensate the photogenerated current, and therefore important to match the correct V_{oc} value. For the bias voltages lower than 0.5 V the recombination current is rather low and the photogenerated current will dominate the *J-V* characteristics. Thus the external G_{sh} might be of lesser importance when observing the illuminated solar cell structure.

3.2 Illuminated structure characteristics

In order to calibrate the CZTSSe solar cell model under illumination, we choose to observe the temperature behaviour of the J_{sc}. This is mainly determined by the collection efficiency of the photogenerated carriers in the SCR. The collection efficiency in a large extend depends on the width of the SCR (Fig. 4), determined by the shallow acceptor traps in the CZTSSe - $N_{tA,CZTSSe}$, while its temperature dependence governs the occupation function *F* of the deeper donor traps $N_{tD,CZTSSe}$ (Fig. 10). Fig. 10 shows the $N_{tA,CZTSSe}$ and $N_{tD,CZTSSe}$ distributions similar to the measured trap densities from Fig. 7, and the occupation function *F* at 310 K and 210 K. The peak values of the trap distributions are not the same as the measured traps, but were rather subjected to the calibration procedure of fitting the *J-V* and *QE* measured and simulated characteristics. At the edge of the SCR the apparent doping p_{SCR} is a result of the compensatory effect of the density of the occupied $N_{tA,CZTSSe}$ and the density of the unoccupied $N_{tD,CZTSSe}$:

$$p_{SCR} = N_{tA,CSZSSe} - (1-F)\cdot N_{tD,CSZSSe}\,. \tag{2}$$

When temperature decreases the E_{fp} moves towards the valence band, what creates more deep donors unoccupied (f_B decreases), and lowers the p_{SCR}.
In Fig. 10 the trap distributions of the model are calibrated to fit the measured short-circuit current density at 310 K. The distributions correlate well with the calculated distributions shown in Fig. 7. On the right axis the occupation functions at two different temperatures are shown in order to explain the temperature dependent collection efficiency and its influence to the short-circuit current.
The temperature decreasing p_{SCR} decreases the SCR width, leading into the lower collection efficiency and lower J_{sc}. Fig. 11 shows the SCR narrowing as the result of the Fermi redistribution according to Fig. 10. The decreased p_{SCR} would normally lead into the wider SCR, if the net charge of the SDL remained constant. This would be the case with the ideal asymmetrical n^+/p junction, resulting from the shallow doping levels. But since the net charge in the SDL originates also from the deep defects, these are then affected by the change of the charge in the CZTSSe layer. Therefore in order to satisfy the Poisson's balance, the lower temperature also leads into the charge redistribution in the SDL layer (omitted for clarity in Fig. 11): the decrement of the negative charge resulting from the less occupied acceptor traps in the CZTSSe layer is balanced by the decrement of the positive charge from the deep defects in the SDL. In the SDL the temperature shift of the Fermi level towards the conduction band makes the deep donor defects less ionized and increases the ionization of the deep acceptors.

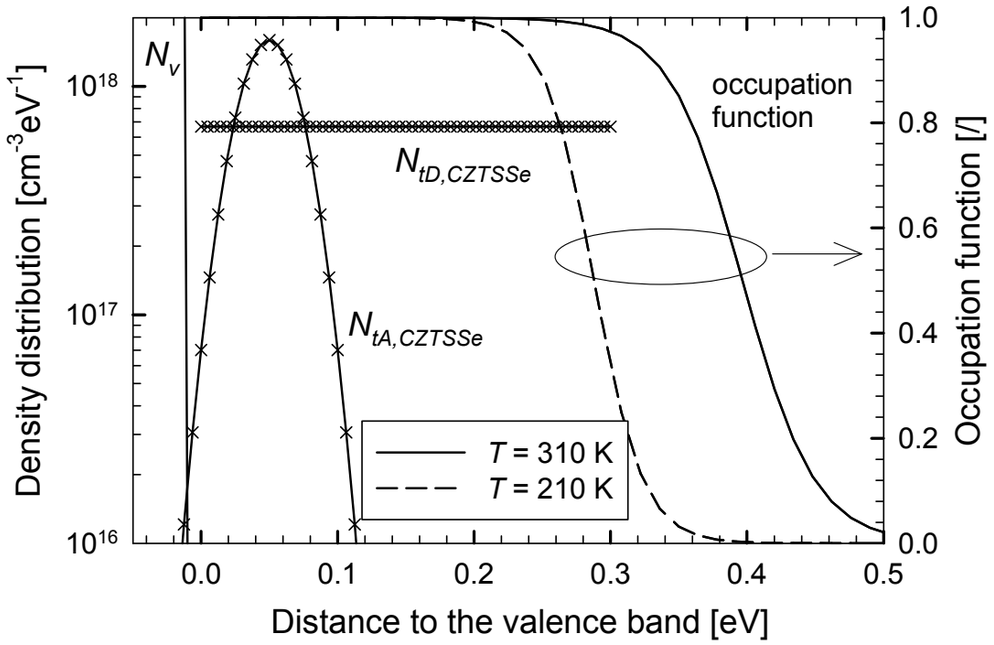

Fig. 10. Trap distributions of the CZTSSe monograin layer 50 nm deep in the SCR from the SDL/CZTSSe heterointerface.

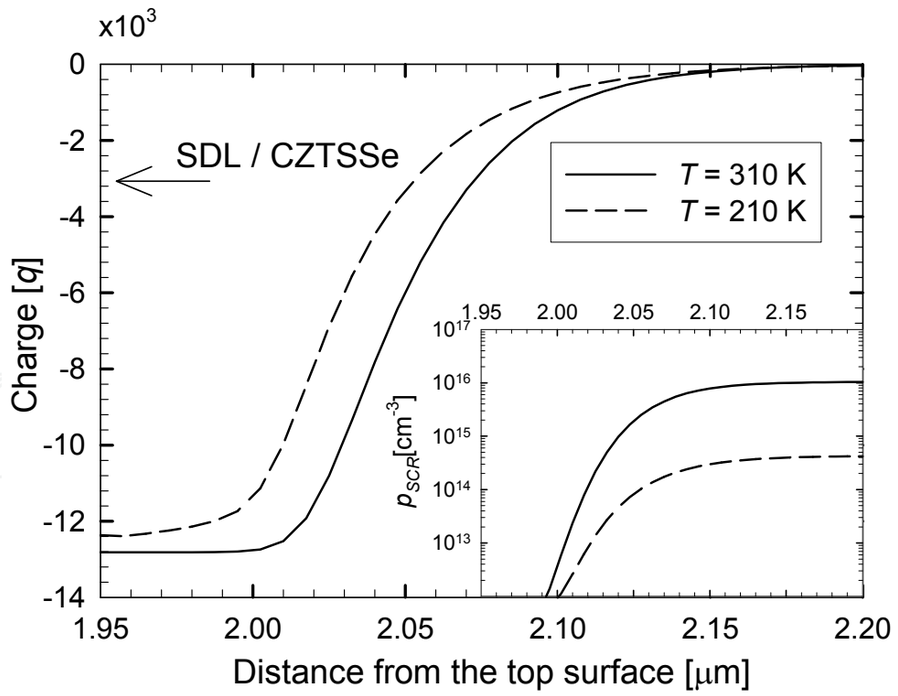

Fig. 11. Space charge region of the CZTSSe layer (q is the electron's charge) and its temperature dependence resulting from the occupation function variation (shown in Fig. 10). On the left, the interface to the SDL is indicated. The inset shows the temperature variation of the apparent doping p_{SCR}.

The modelled SCR width of approximately 0.2 μm and the p_{SCR} concentration of 10^{16} cm^{-3} at 310 K agree well with the respective measured values which equal to 0.18 μm and 2.6x10^{16} cm^{-3}, as observed from Fig. 4. Similarly well agrees the temperature correlation between the p_{SCR} and the SCR width: with the increasing p_{SCR} also the increasing SCR width is observed. In the measurement this correlation is indicated with the triangles (Fig. 4). However the corresponding temperatures do not comply: in the measurement the 320 K triangle corresponds to the lowest p_{SCR} and the 220 K triangle corresponds to the highest p_{SCR}. One should indeed always take care about the width of the SCR calculated in the apparent doping density analysis. There, the following formula is used to calculate the SCR width:

$$W_{SCR} = \frac{\varepsilon}{C}, \tag{3}$$

where ε is the permittivity and C is the capacitance. This formula however only holds if the capacitance is governed by the depletion, and not by filling and emptying of deep states. As can be seen in Fig. 6 the capacitance is indeed governed by defects rather than depletion at f=10kHz.

Table 2 summarizes the calibrated material parameters. The parameters which were the subject of calibration are denoted bold, while the dash corresponds to the parameter for which we used the value 0. In the reality this would correspond to a very low value. Other material parameters are similar as in (Černivec et al., 2008). The effective density of states is calculated from the corresponding effective masses (Sze & Ng, 2007).

	ZnO:Al	i-ZnO	CdS	SDL	CZTSSe
W [μm]	1.6	0.2	0.05	0.1	60
m_e [m_0]	0.27	0.27	0.27	0.09	0.09
m_h [m_0]	0.78	0.78	0.78	0.73	0.73
N_D [cm^{-3}]	10^{18}	10^{18}	10^{18}	-	-
N_A [cm^{-3}]	-	-	-	-	-
E_g [eV]	3.3	3.1	2.4	1.4	1.4
E_χ [eV]	4.0	4.0	4.0	4.0	4.0
E [ε_0]	9.0	9.0	9.0	13.6	13.6
μ_e [cm^2/Vs]	100	100	100	**40**	**8**
μ_h [cm^2/Vs]	25	25	25	**15**	**1.5**
N_{tA} [cm^{-3}/eV]	-	-	-	**4x10^{17}**	**8x10^{16}**
E_{tA} [eV]	-	-	-	**0.7**	**0.05**
σ_{nA} [cm^2]	-	-	-	**2x10^{-15}**	**2x10^{-15}**
σ_{pA} [cm^2]	-	-	-	**8x10^{-13}**	**8x10^{-13}**
e_{tA} [eV]	-	-	-	**0.1 (step)**	**0.02 (gauss)**
N_{tD} [cm^{-3}/eV]	-	-	-	**8x10^{19}**	**7x10^{17}**
E_{tD} [eV]	-	-	-	**0.7**	**0.15**
σ_{nD} [cm^2]	-	-	-	**8x10^{-14}**	**10^{-14}**
σ_{pD} [cm^2]	-	-	-	**2x10^{-15}**	**10^{-15}**
e_{tD} [eV]	-	-	-	**0.1 (step)**	**0.3 (step)**

Table 2. Material parameters of the CZTSSe MGL monograin layer solar cell.

4. Analysis of the model

Fig. 12 shows the measured and simulated *J-V* characteristics of the CZTSSe MGL solar cell. The measured characteristics were obtained from the *I-V* characteristics normalized to the contacting area of the solar cell equal to A = 4.81 mm². Here we used the assumptions i) and ii) as defined in 3. Since the CZTSSe monograins shape in the spherical forms this means that the real current density varies throughout the structure. In the simulated *J-V* characteristics at 310 K we also took into account the S_{FF} as the assumption iii). This means that the J_{sc} obtained by using the parameters from Table 2 would in fact be larger by this factor.

In Fig. 12 we can observe a very good agreement of the measured and simulated *J-V* characteristics at 310 K while the simulation at 210 K exhibits a discrepancy in all solar cell output parameters. A possible reason for the non-matched J_{sc} at 210 K could be that in the modelling we did not account for the temperature dependent mobility, which could be the case as seen from the van der Pauw measurement of the monograin tablet (Fig. 5).

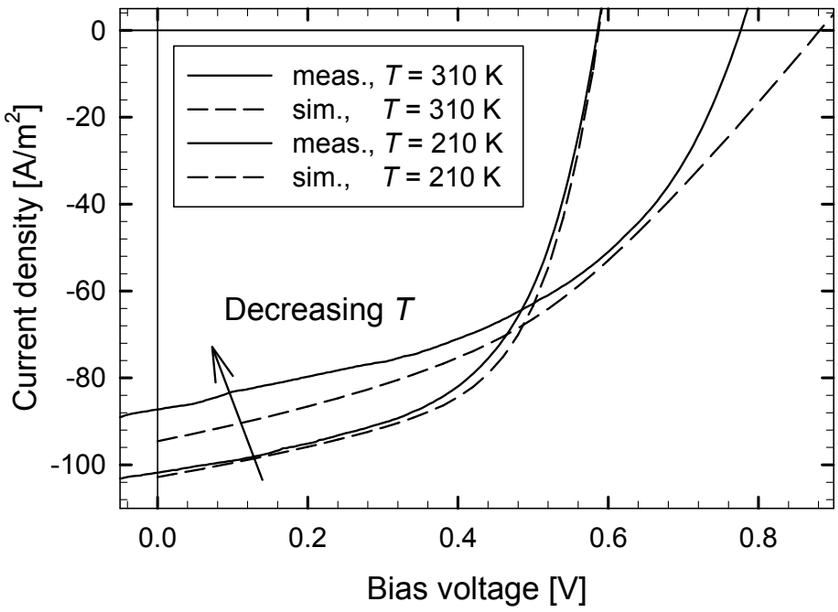

Fig. 12. Comparison of the measured and simulated *J-V* characteristics of the AM1.5 illuminated CZTSSe monograin solar cell.

Dashed lines in Fig. 12 represent the simulation and the arrow indicates temperature decrement. The short-circuit current and the open-circuit voltage trends are well correlated while their absolute value deviation at the low temperature indicate the necessity to include the temperature dependent mobility and the tunnelling enhanced recombination, respectively. At 210 K a significant mismatch also occurs with the V_{oc}. This leads us to the conclusion that it is not merely the SRH recombination (Sze & Ng, 2007) in the SDL layer that limits the V_{oc}, but there should also be present other recombination mechanisms which are less thermodynamically affected, namely the tunnelling enhanced recombination (Dumin & Pearson, 1965). The tunnelling enhanced recombination would reduce the rate of the V_{oc}-T change.

The optical simulations were performed using the Sun*Shine* simulator (Krč et al., 2003) which takes as an input a layered structure with the wavelength dependent complex refraction index coefficients, which comprise the real part $n(\lambda)$, called refractive index, and the complex part $k(\lambda)$ known as the extinction coefficient. Both are defined in for each layer. For the monograin material we used the complex refraction index coefficients as obtained by Paulson (Paulson et al., 2003) for the thin film $Cu(In_{1-x}Ga_x)Se_2$ alloy with the $x = 0.66$. This corresponds to the energy gap of 1.41 eV. The layer's interfaces were described using the roughness coefficient – σ_{rms}. In our case we set the σ_{rms} equal to 100 nm at all interfaces. Simulation of the external quantum efficiency (Fig. 13) shows a good agreement between the measured *QE* and the simulated *QE* in the shorter wavelengths region, while in the middle wavelengths there seems to exist some discrepancy – most probably due to the discrepancy between the measured and modelled $\mu_{h,CZTSSe}$. The cut-off wavelengths are well pronounced at both temperatures and correspond to the band-gap of 1.4 eV. In the long wavelength region (λ > 900 nm) the non-vanishing plateau of the simulated *QE* points to a mismatch in the absorption properties of the thin film CIGS and the monograin layer CZTSSe materials.

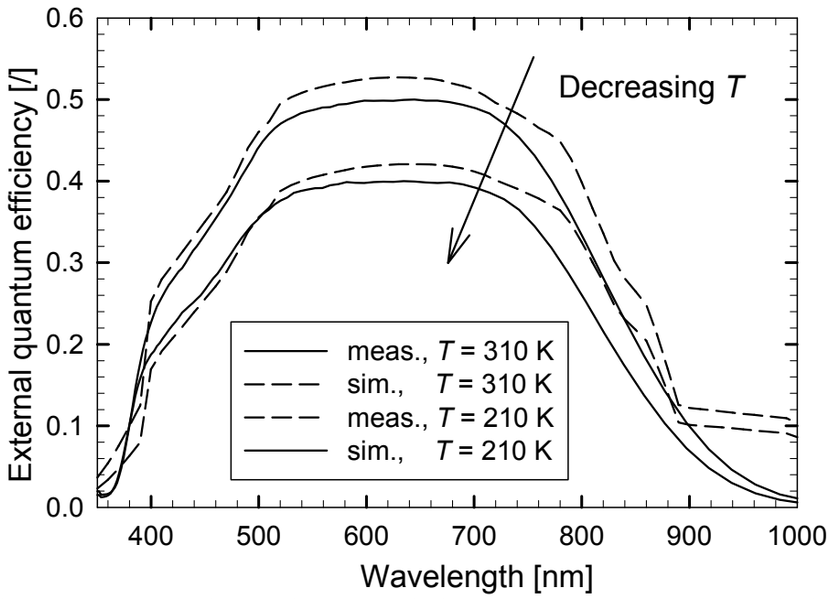

Fig. 13. Comparison of the measured and simulated external quantum efficiency of the AM1.5 illuminated CZTSSe monograin solar cell.

In Fig. 13 dashed lines represent the simulation and the arrow indicates temperature decrement. The non-vanishing plateau of the simulation originates from the mismatch in the absorption properties of the thin film CIGS (used in the simulation) and the monograin layer CZTSSe materials.

Both, measured and simulated *QE* show that the temperature change does not affect their shape, which inclines us to a conclusion that most of the photogenerated carriers recombine in the SDL and at the SDL/CZTSSe interface. This fact can as well be observed from the cumulative recombination profile (not shown here).

The absorptance simulations show that if all photogenerated carriers originating from the photon flux absorbed in the CZTSSe layer were extracted, the J_{sc} would equal to 37.7 mA/cm². Taking into account the S_{FF} the latter would reduce to a 29.4 mA/cm². This value

is still about 3 times larger than the measured (simulated) J_{sc} at 310 K, showing tremendous possibilities in improvement of the collection efficiency of the monograin CZTSSe absorber.

5. Conclusion

We have set up the baseline model of the $Cu_2SnZn(Se,S)_4$ monograin layer solar cell, which is able to predict the *J-V* characteristics and the external *QE* of the AM1.5 illuminated MGL solar cell in the temperature range from 310 K to 210 K. The model comprises following material properties:
i) in between the CdS and CZTSSe layers, the highly defective region called the surface defect layer – SDL, comprising a high concentrations of the mid-gap donor defects and a lower concentration of the mid-gap acceptor defects;
ii) in the CZTSSe monograin layer the narrow Gaussian distribution of shallow acceptor traps at 0.05 eV above the valence band and the wider distribution of the compensatory donor traps extending at least 0.3 eV deep into the energy band, relative to the valence band;
iii) energy gap of the CZTSSe monograin material equals to 1.4 eV, width of the SCR at 310 K equals to 180–200 nm and the concentration of the apparent doping p_{SCR} is in the range from $1x10^{16}$ cm^{-3} to $2x10^{16}$ cm^{-3}.
Low *FF* can be attributed to the low CZTSSe hole mobility, which equals to 1.5 cm^2/Vs, and to the low apparent doping p_{SCR}, which originates from the compensatory effect of the shallow acceptors and deeper donors. Comparison of the flux absorbed in the CZTSSe monograin absorber and the three times lower actual current density of the extracted carriers shows us that further possibilities may reside in the shaping of the collection efficiency of the monograin absorber and/or in the additional passivation of the CdS/CZTSSe interface. Since the former is mainly attributed to the SCR this might not be an easy technological task. Whether these limiting properties are the result of the necessary surface engineering prior to the formation of the CdS/CZTSSe monograin heterojunction or they simply originate from the physical properties of the structure's materials, we were be not able to determine at this point.

6. Acknowledgments

Authors would like to thank prof. dr. Jüri Krustok, Tallinn University of Technology, for his objective criticism which helped to improve the quality of this work. We also thank prof. dr. Marko Topič, University of Ljubljana, for his approval on the use of the simulation software Aspin2 and Sun*Shine*.

7. References

Altosaar, M.; Jagomägi, A.; Kauk, M.; Krunks, M.; Krustok, J.; Mellikov, E.; Raudoja, A. & Varema, T. (2003). Monograin layer solar cells. *Thin Solid Films*, Vol. 431-432, pp. 466-469, ISSN 0040.6090

Altosaar, M.; Danilson, M.; Kauk, M.; Krustok, J.; Mellikov, E.; Raudoja, J.; Timmo, K. & Varema, T. (2005). Further development in CIS monograin layer solar cells technology. *Solar Energy Materials & Solar Cells*, Vol. 87, pp. 25-32, ISSN 0927.0248

Breitenstein, O.; Altermatt, P.; Ramspeck, K. & Schenk, A. (2006). The origin of ideality factors N>2 of shunt and surfaces in the dark I-V curves of SI solar cells, *Proceedings*

of the 21st European Photovoltaic Solar Energy Conference, pp. 625-628, Dresden, Germany.

Burgelman, M. & Nollet, P. (2005). Admittance spectroscopy of thin film solar cells. *Solid State Ionics*, Vol. 176, pp. 2171-2175, ISSN 0167.2738

Černivec, G.; Jagomägi, A.; Smole, F. & Topič, M. (2008). Numerical and experimental indication of thermally activated tunnelling transport in CIS monograin layer solar cells. *Solid State Electronics*, Vol. 52, pp. 78-85, ISSN 0038.1101

Dumin, D.J. & Pearson, G.L. (1965). Properties of gallium arsenide diodes between 4.2 and 300 K. *Journal of Applied Physics*, Vol. 36, No. 11, pp. 3418-3426, ISSN 0021.8979

Kosyachenko, L. (2010). Efficiency of thin film CdS/CdTe Solar Cells, In: *Solar Energy,* R.D. Rugescu, (Ed.), 105-130, InTech, ISBN 978-953-307-052-0, Vukovar, Croatia.

Krč, J.; Smole, F. & Topič M. (2003). Analysis of light scattering in amorphous Si:H solar cells by one-dimensional semi-coherent optical model. *Progress in Photovoltaics: Research and Applications*, Vol. 11, pp. 15-26, ISSN 1062.7995

Paulson, P.D.; Birkmire, R.W. & Shafarman, W.N. (2003). Optical characterization of $CuIn_{1-x}Ga_xSe_2$ alloy thin films by spectroscopic ellipsometry. *Journal of Applied Physics*, Vol. 94, No. 2, pp. 879-888, ISSN 0021.8979

Sah, C.T.; Noyce, R.N. & Shockley, W. (1957). Carrier generation and recombination in p-n junctions and p-n junction characteristics. *Proceedings of the Institute of Radio Engineers*, Vol. 45, No. 9, pp. 1228-1243, ISSN 0731.5996

Schenk, A. & Krumbein, U. (1995). Coupled defect-level recombination: Theory and application to anomalous diode characteristics. *Journal of Applied Physics*, Vol. 78, No. 5, pp. 3185-3192, ISSN 0021.8979

Schockley, W.; Read, W.T. (1952). Statistics of the recombination of holes and electrons. *Physical Review*, Vol. 87, pp. 835-842

Selberherr, S. (1984). *Analysis and simulation of semiconductor devices*, Springer Verlag, ISBN 978.0387818009, Vienna, Austria

Sze, S.M. and Ng, K.K. (2007). *Physics of semiconductor devices*, John Wiley & Sons, ISBN 9971.51.266.1 , New Jersey, USA

Topič, M.; Smole, F. & Furlan, J. (1996). Band-gap engineering in $CdS/Cu(In,Ga)Se_2$ solar cells. *Journal of Applied Physics*, Vol. 79, No. 11, pp. 8537-8540, ISSN 0021.8979

Van der Pauw, L.J. (1958). A method of measuring specific resistivity and Hall effect of discs of arbitrary shape. *Phillips Research Reports*, Vol. 13, pp. 1-9, ISSN 0031.7918

Walter, T.; Herberholz, R.; Müller, C. & Schock H.W. (1996). Determination of defect distributions from admittance measurements and application to $Cu(In,Ga)Se_2$ based heterojunctions. *Journal of Applied Physics*, Vol. 80, No. 8, pp. 4411-4420, ISSN 0021.8979

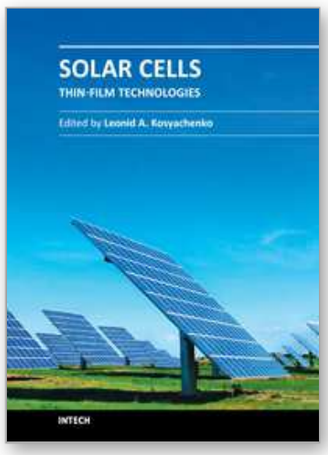

Solar Cells - Thin-Film Technologies

Edited by Prof. Leonid A. Kosyachenko

ISBN 978-953-307-570-9
Hard cover, 456 pages
Publisher InTech
Published online 02, November, 2011
Published in print edition November, 2011

The first book of this four-volume edition is dedicated to one of the most promising areas of photovoltaics, which has already reached a large-scale production of the second-generation thin-film solar modules and has resulted in building the powerful solar plants in several countries around the world. Thin-film technologies using direct-gap semiconductors such as CIGS and CdTe offer the lowest manufacturing costs and are becoming more prevalent in the industry allowing to improve manufacturability of the production at significantly larger scales than for wafer or ribbon Si modules. It is only a matter of time before thin films like CIGS and CdTe will replace wafer-based silicon solar cells as the dominant photovoltaic technology. Photoelectric efficiency of thin-film solar modules is still far from the theoretical limit. The scientific and technological problems of increasing this key parameter of the solar cell are discussed in several chapters of this volume.

InTech Europe
University Campus STeP Ri
Slavka Krautzeka 83/A
51000 Rijeka, Croatia
Phone: +385 (51) 770 447
Fax: +385 (51) 686 166
www.intechopen.com

InTech China
Unit 405, Office Block, Hotel Equatorial Shanghai
No.65, Yan An Road (West), Shanghai, 200040, China
中国上海市延安西路65号上海国际贵都大饭店办公楼405单元
Phone: +86-21-62489820
Fax: +86-21-62489821

IntechOpen